EFFECT OF MIXED REFRIGERANT COMPOSITION ON PERFORMANCE OF AN AUTO-CASCADE REFRIGERATION SYSTEM USING R600A/R1150/R14

Wenlian YE[1,2,]*, Yang LIU[1], Lulu HU[2,3], Peng YANG[4], Yingwen LIU[4]

[1]Key Laboratory of Fluid Machinery and System, Gansu Province, College of Energy and Power Engineering, Lanzhou University of Technology, Lanzhou, Gansu, 730000 PR China

[2]Zhe Jiang AMA&HIEN Technology Co., Ltd, Yueqing, Zhejiang, 325600 PR China

[3]School of Mechanical Engineering, Jiangsu University of Technology, Changzhou, Jiangsu, 213100 PR China

[4]Key Laboratory of Thermo-Fluid Science and Engineering of MOE, School of Energy and Power Engineering, Xi'an Jiaotong University, Xi'an, Shaanxi 710049 PR China

Corresponding author; E-mail: ywl-315@lut.edu.cn

A mathematical model based on energy and exergy methods is established to analyze the performance of an auto-cascade refrigeration system at varying compositions of the mixed refrigerants, condensation temperature, evaporation temperature, and vapor quality at the condenser outlet. Furthermore, grey correlation theory is employed to assess the correlation degrees between refrigerant mass fractions and system performance, enabling the identification of the state that has the greatest impact on the output parameters. It has been concluded that while maintaining a constant mass fraction of R600a, an increase in the mass fraction of R1150 (state 1) leads to a higher cooling capacity but a decrease in exergy efficiency. The performance decreases with the increase of the R600a mass fraction (state 2) as the R1150 mass fraction is unchanged. When the component of R14 is constant while the other two components R600a/R1150 vary (state 3), and the COP exists as the optimal value. The mixture of R600a/R1150/R14 with a mass fraction of 0.5:0.2:0.3 has better performance at COP of 0.5027 and exergy efficiency of 29.43 % under a condensation temperature of 30℃. Based on the results of the grey correlation degree, the greatest factor in cooling capacity is state 1, while the COP and exergy efficiency are primarily controlled by state 3.

Keywords: *Auto-cascade; refrigeration cycle; grey correlation degree*

1. Introduction

With the increasing requirement for a low-temperature environment in biomedical science, rapid freezing, and vaccine preservation, it is urgent to develop ultra-low-temperature refrigerators with temperatures below -90 ℃ [1]. The traditional single-stage compression refrigeration system is limited by the high-pressure ratio, high discharge temperature, and low efficiency of the compressor and is mostly used to obtain low temperatures between -20 ℃ and -40 ℃ [2]. Multi-stage compression refrigeration systems with a single medium-temperature refrigerant can obtain low temperatures above -40 ℃ under the limitation of low evaporation pressure. So, cascade refrigeration cycles and auto-cascade refrigeration cycles (ACR) have been widely used in applications from -80°C down to

cryogenic temperatures [3]. However, two or more single-stage circuits are connected in the cascade refrigeration system (CRS), which requires two or more compressors, resulting in an increase in the initial investment [4]. Compared with traditional multi-stage compression and CRS, the ACR systems can obtain low refrigeration temperatures from -40 ℃ to -160 ℃ adopting only one compressor and a set of zeotropic mixed refrigerants with different compositions [5]. Consequently, the researchers have focused their attention on the ACR cycles.

To improve the performance of the ACR systems, many researchers have investigated the complicated cycle analysis of the ACR systems, consisting of cycle configuration improvement [6]. optimization of the mixed refrigerant compositions [7], etc. In terms of the optimization of the refrigerant compositions, Wang *et al.* [8] investigated the performance of a single-stage system operating with two vapor-liquid separators and six binary refrigerants, and the results showed that the refrigerants R23/R236fa and R170/R600 with the mol fraction at 0.55 for R23 and R170 were the best compositions. Sivakumar *et al.* [9] applied R290/R23/R14 and R1270/R170/R14 to perform the performance and the energic analysis, and the results illustrated that R290/R23/R14 with the mass fraction of 0.218:0.346:0.436 performed better. Rui *et al.* [10] investigated the performance of the ternary mixture R600a/R23/R14 of an ACR by changing the compositional ratio. The results illustrated that the mass fraction of 0.35:0.30:0.35 was recommended. A modified refrigeration cycle with a Linde-Hampson refrigeration system and an ACR system using two refrigerant combinations of R1234yf/R32 and R170/R14/R50 was carried out by Qin *et al.* [11]. The results indicated that the exergy efficiency and COP were 15.18% and 0.1438, as the R170/R14/R50 composition was 0.52:0.22:0.26. Liu *et al.* [12] proposed a novel ejector-enhanced ACR cycle using R290/R170 with different refrigerant compositions and obtained the best mass fraction of R290.

As described in the literature above, many researchers have focused on the ACR system characteristics of the alternative refrigerants, consisting of R236fa/R23, R290/R170, R600/R170, R600a/R170, R744/R290, R600a/R1150 [13], etc. Besides, Liu *et al.* [14] focused on evaluating and analyzing the ACR's performance with the refrigerants R600a/R1150/R14 using grey correlation theory and response surface methodology. The interactive influences that had great impacts on the performance were illustrated, and the correlation degree between the operating conditions and ACR's performance was obtained. Ye *et al.* [15] demonstrated the multi-objective optimization of an ultra-low temperature CRS through response surface methodology and the desirability approach, and the optimized parameter combinations of operating parameters were given. However, the refrigerant mass fractions were fixed in reference 14, while the response surface methodology for multi-objective optimization in a CRS consisting of a low-temperature circuit and a high-temperature circuit to identify the optimized results was employed in reference 15. In addition, there is no published literature to show the impacts of the mass fractions on the ACR's performance for ultra-low temperature refrigerators operating with R600a as the high boiling refrigerant, R1150 as the middle boiling refrigerant, and R14 as the low boiling refrigerant. Furthermore, it is difficult to find literature indicating which state (state 1: the composition of R600a is constant but the initial mass fractions of R1150 and R14 vary; state 2: the composition of R1150 keeps constant but the initial mass fractions of R600a and R14 change; state 3: the composition of R14 is not changed while the initial mass fractions of R600a and R1150 change) has the greatest or least effects on the ACR's performance. Therefore, it is necessary to find out the relationship between the input and output parameters when the mass fractions of R600a, R1150, and R14 are in different states, and evaluate the correlation

degree between the three states and the output parameters. Thus, this paper aims to conduct the energy and exergy analysis for the three states under different operating conditions and find an effective approach to evaluating the correlation degree between the states and the ACR's performance. The results will provide a theoretical guide for adjusting the mass fraction of the refrigerants in the ACR system. Furthermore, we can identify the state that exerts the greatest influence on performance by applying the grey correlation theory. This approach facilitates the adjustment of the initial mass fraction of refrigerants in subsequent experiments, thereby providing valuable guidance for future research on the performance improvement of an ultra-low-temperature refrigeration system.

2. Mathematical model

2.1. Selection of the refrigerants

Generally, the ACR's performance is greatly influenced by the characteristics of mixed refrigerants. In the coming decades, refrigerants containing HFCs will be phased out, favoring those with low ODP and GWP. Table 1 summarizes the key properties of the candidate refrigerants. Among high-boiling refrigerants, R600a stands out with its zero ODP and low GWP of 20, rendering it a preferred option for environmentally friendly freezers and refrigerators. In comparison to R290, R600a poses a significantly reduced explosion risk and exhibits lower flammability. For middle-boiling refrigerants, R1150 is selected for its low ODP, GWP, and safety grade of A3. Among low-boiling refrigerants, R14 is preferred due to its low ODP, minimal flammability, and lower boiling temperature. Taking into account its application background, temperature range, and other relevant characteristics, the combination of R600a, R1150, and R14 is selected for the ACR system.

Table 1. Key properties of the refrigerants in ACR systems[14]

Refrigerant	Chemical formula	ODP	GWP	Normal boiling temperature at one Atm.(K)	Critical temperature (K)	Critical pressure (KPa)
R600a	C_4H_{10}	0	20	261.42	407.81	3.627
R134a	CH_2FCF_3	0	1300	247.08	374.21	4.059
R22	$CHFCL_2$	0.055	1700	232.34	369.3	4.99
R290	$CH_3CH_2CH_3$	0	~20	231.04	369.89	4.251
R744	CO_2	0	1	216.59	304.13	7.377
R23	CHF_3	0	12100	191.13	299.29	4.832
R170	CH_3CH_3	0	20	184.57	305.32	4.8722
R1150	CH_2=CH_2	0	20	169.38	282.35	5.042
R14	CF_4	0	5700	145.1	227.51	3.75
R50	CH_4	0	24.5	111.67	190.56	4.6

2.2. Cycle and system description

The schematic diagram of the refrigeration cycle with a vapor-liquid phase separator is displayed in Fig. 1. In this ACR system, a mixture of R600a/R1150/R14 is utilized. The main component with R600a is used in the high-temperature loop while the main refrigerant, R1150/R14, is applied in the low-temperature loop. This system mainly consists of a compressor with suction at point 1 and discharging at point 2, a finned tube condenser, a cascade heat exchanger (CHX), two expansion valves (EVs), two inner heat exchangers (IHXs), and an evaporator. The separator is

applied to obtain the separation of low-boiling refrigerant. The corresponding *p-h* diagram of the ACR cycle is shown in Fig. 2. Points 1-2: the compression process of the mixed refrigerant in the compressor; Points 2-3: the condensation process in the condenser; Points 3-12 and 3-4: the process of separating a mixed refrigerant into liquid rich in high boiling point components and gas rich in low boiling point components in a gas-liquid separator; Points 12-13: the throttling process of a liquid rich in high boiling components in EV-1; Points 4-5: the condensation process of gases rich in low boiling components in the CHX; Points 7-8: the throttling process of a liquid rich in low boiling components in EV-2; Points 8-9: the evaporation process of refrigerants rich in low boiling components in the evaporator; Points 13-11 and 10-11: the mixing process of high boiling and low boiling working fluids. Two internal heat exchangers, namely IHX-1 and IHX-2, have been integrated into the system to lower the inlet temperature of the evaporator.

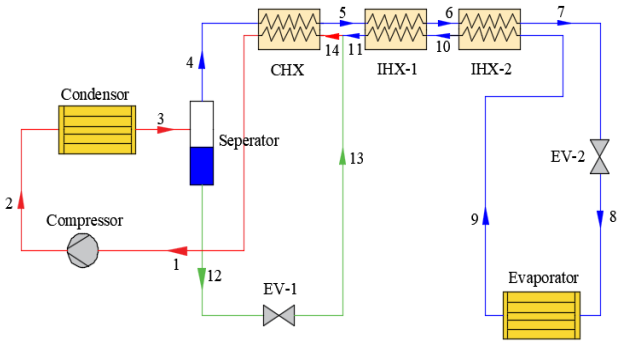

Fig. 1. Schematic diagram of the ACR system

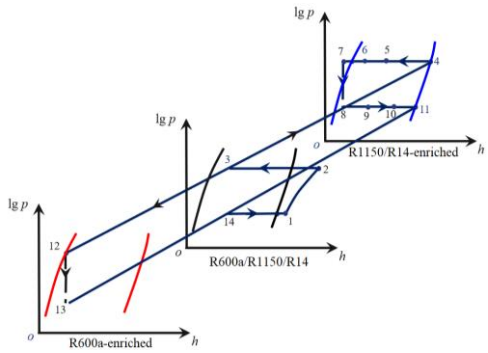

Fig. 2. Pressure-enthalpy diagram

2.3. Cycle system modeling

Based on the working principle of the ACR system and the first law of thermodynamics, the performance is theoretically evaluated. The assumptions are made for the model as follows:(1) All components of the ACR system are assumed to be in a steady state and steady flow process. (2) The compression process in the compressor is adiabatic and irreversible, and the expansion processes in EV-1 and EV-2 are isenthalpic. (3) All the pressure drops and heat losses in the ACR system are neglected. (4) The exergy analysis takes p_0=101 kPa and t_0=25 ℃ as the standard conditions.

According to the assumptions, the conservation equations of mass and energy are established, as listed in Tab. 2.

Table 2. The conservation equations of the mass and energy

Components	Mass conservation	Energy conservation
Compressor	$m_1=m_2$	$W_{com}=m_1(h_2-h_1)=m_1(h_{2,is}-h_1)/\eta_{com}$
Condenser	$m_2=m_3$	$Q_c=m_2(h_2-h_3)$
Evaporator	$m_8=m_9$	$Q_e=m_9(h_9-h_8)$
Separator	$m_3=m_4+m_{12}$	$m_3h_3=m_4h_4+m_{12}h_{12}$
CHX	$m_4=m_5$, $m_1=m_{14}$	$m_4(h_4-h_5)=m_1(h_1-h_{14})$
IHX-1	$m_5=m_6$, $m_{10}=m_{11}$	$h_5-h_6=h_{11}-h_{10}$
IHX-2	$m_6=m_7$, $m_9=m_{10}$	$h_6-h_7=h_{10}-h_9$
EV-1	$m_{12}=m_{13}$	$h_{12}=h_{13}$
EV-2	$m_7=m_8$	$h_7=h_8$

In Tab. 2, the subscript ‘is’ represents the isentropic process; η_{com} can be expressed as [16]:

$$\eta_{\text{com}} = 0.874 - 0.0135 r_{\text{com}} = 0.874 - 0.0135(p_2 / p_1) \quad (1)$$

The coefficient of performance (COP) of the ACR cycle is described as:

$$COP = Q_{\text{e}} / W_{\text{com}} \quad (2)$$

The exergy analysis offers a good method to assess the irreversible loss of each component. The exergy destruction rate of each component is shown in Tab. 3. In Tab. 3, ΔT is set to be 5K.

Table 3. The exergy destruction rate of the components

Components	Exergy conservation
Compressor	$Ex_{\text{d,com}} = m_1 T_0 (s_2 - s_1)$
Condenser	$Ex_{\text{d,c}} = m_2((h_2 - h_3) - T_0(s_2 - s_3)) - Q_{\text{c}}(1 - \frac{T_0}{T_c})$
Evaporator	$Ex_{\text{d,e}} = m_8((h_8 - h_9) - T_0(s_8 - s_9)) + Q_{\text{e}}(1 - \frac{T_0}{T_{\text{e}} + \Delta T})$
CHX	$Ex_{\text{d,CHX}} = m_4((h_4 - h_5) - T_0(s_4 - s_5)) + m_1((h_{14} - h_1) - T_0(s_{14} - s_1))$
IHX-1	$Ex_{\text{d,IHX1}} = m_5((h_5 - h_6) - T_0(s_5 - s_6)) + m_{11}((h_{10} - h_{11}) - T_0(s_{10} - s_{11}))$
IHX-2	$Ex_{\text{d,IHX2}} = m_6((h_6 - h_7) - T_0(s_6 - s_7)) + m_9((h_9 - h_{10}) - T_0(s_9 - s_{10}))$
EV-1	$Ex_{\text{d,exp1}} = m_{12} T_0 (s_{13} - s_{12})$
EV-2	$Ex_{\text{d,exp2}} = m_7 T_0 (s_8 - s_7)$

Therefore, the total exergy destruction rate and exergy efficiency of the ACR system are given:

$$Ex_{\text{d}} = Ex_{\text{d,com}} + Ex_{\text{d,c}} + Ex_{\text{d,e}} + Ex_{\text{d,CHX}} + Ex_{\text{d,IHX1}} + Ex_{\text{d,IHX2}} + Ex_{\text{d,exp1}} + Ex_{\text{d,exp2}} \quad (3)$$

$$n_{ex} = 1 - \frac{E_{x_{\text{d}}}}{W_{\text{com}}} \quad (4)$$

2.4. Operating conditions and solving procedure

To conduct a parametric analysis on the thermodynamic characteristics of the ACR across various working conditions, the operating parameters are presented in Tab. 4. As shown in Tab. 4, the ranges of the six input variables are given, and the other three parameters are set as constants. Based on the assumptions in Section 2.3 and the operating conditions, the thermodynamic model of the ACR is built using Hysys software. The output parameters, such as the refrigerating capacity (Q_{e}), the coefficient of performance (COP), the total exergy destruction rate (Ex_{d}), and exergy efficiency, are determined by varying the input parameters. In our calculation, the separation process is equilibrious at the specified conditions, and the concentrations of vapor and liquid obtained from the separator are determined using the properties provided by the REFPROP database.

Table 4. Operating conditions

Parameter	Unit	Values/Ranges
Mass fraction of R600a (Z_{R600a})	/	0.4~0.6
Mass fraction of R1150 (Z_{R1150})	/	0.2~0.4
Mass fraction of R14 (Z_{R14})	/	0.1~0.3
Evaporation temperature (t_{e})	℃	-100~-90
Condensation temperature (t_{c})	℃	26~34
Vapor quality of the condenser outlet (x_{c})	/	0.7~0.8
Vapor quality of the evaporator outlet (x_{e})	/	0.4
Vapor superheat at the compressor inlet (Δt)	℃	5

Cold temperature difference of CHX (t_5-t_4)	℃	30

3. Grey correlation degree method

The basic idea of the grey correlation degree is to measure the degree of association according to the similarity and trend among the factors, and the size of the similarity degree of curves is taken as the weight scale of correlation [17, 18].

It is assumed that $X_0 = \{\varepsilon_0(k) k = 1, 2, 3, ..., n\}$ represents the reference sequence and $X_i = \{\varepsilon_i(k) k = 1, 2, 3, ..., n, i = 1, 2, 3, ..., m\}$ represents the comparison sequence. m and n denote the number of targets, and k denotes the time. In this paper, the initial mass fractions of R600a, R1150, and R14 are selected as the comparison sequences, and the refrigerating capacity (Q_e), the coefficient of performance (COP), the total exergy destruction rate (Ex_d), and exergy efficiency (n_{ex}) are the comparison sequences. Therefore, the degree of grey correlation is given as:

$$\xi_i(k) = \frac{\min_i \min_k |x_0(k) - x_i(k)| + \rho \max_i \max_k |x_0(k) - x_i(k)|}{|x_0(k) - x_i(k)| + \rho \max_i \max_k |x_0(k) - x_i(k)|} \tag{5}$$

$$\gamma_i = \frac{1}{n} \sum_{k=1}^{n} \xi_i(k), k = 1, 2, ..., n \tag{6}$$

4. Results and discussions

4.1. Performance at varying Z_{R1150} and Z_{R14}

Figure 3 displays the cooling capacity (Q_{evap}), COP, exergy destruction rate (E_{xd}), and exergy efficiency (n_{ex}) with respect to the different Z_{R1150} and Z_{R14} at five condensation temperatures t_c. It is clear from Fig. 3 that E_{xd} increases linearly as Z_{R1150} increases or Z_{R14} decreases. Compared to other parameters, the rate of increase in Q_e is relatively small. When t_c is 26 ℃, Q_e is increased by 7.8% with the increasing Z_{R1150}. But COP and n_{ex} decrease. This is because the mass flow of the low-boiling point refrigerants at state point 4 increases as Z_{R1150} increases when x_c is fixed. In addition, the inlet temperature of the evaporator decreases as Z_{R1150} varies from 0.2 to 0.4 while t_e and the vapor quality at the evaporator outlet remain constant, causing a gradual increase in Q_e. The increase in Q_e is smaller than the W_{com} of the compressor, thus COP shows a decreasing trend. Within the given Z_{R1150}, Q_e, COP, E_{xd}, and n_{ex} vary from 113.3~121.8 W, 0.3885~0.2355, 211.4~428.1 W, and 24.4~14.79 % as t_c is 30 ℃. As illustrated in Fig. 3, the increase in t_c has a negative impact on performance. It can be seen that the COP, Q_e, and n_{ex} present a downward trend, while E_{xd} increases as Z_{R14} remains constant.

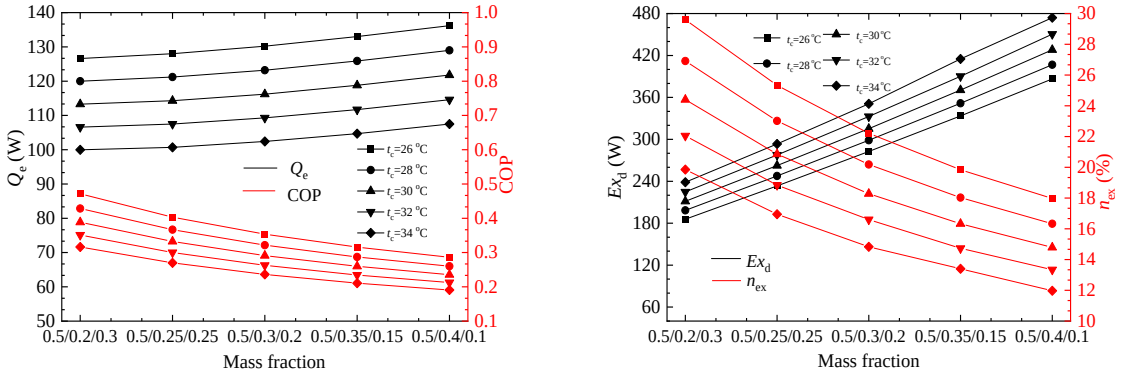

(a) Variations of Q_e and COP *(b) Variations of Ex_d and n_{ex}*

Fig. 3. Variations of output parameters with Z_{R1150} and Z_{R14} at different t_c

Figure 4 shows the variations of Q_e, COP, E_{xd}, and n_{ex} at different Z_{R1150} and Z_{R14} at the five t_e. It can be seen that with the increase of Z_{R1150} (or the decrease of Z_{R14}), Q_e and E_{xd} increase, but COP and n_{ex} decrease. The variation trend of various parameters is consistent with that in Fig. 3. As t_e increases from -100 ℃ to -90 ℃, E_{xd} shows a remarkable decrease, while the COP, Q_e and E_{xd} increase linearly. The recommended values of COP and n_{ex} at a t_e of -90 ℃ are observed for the combination (Z_{R600a}: Z_{R1150}: Z_{R14}=0.5:0.2:0.3) as 0.5027 and 29.43 %. This is the reason that the value of the p_{out} is related to the condensation temperature, the mass fraction of the refrigerants, and the vapor quality at the condenser outlet, which are set to constant values during the simulation. Thus, the p_{out} remains constant as the t_e varies.

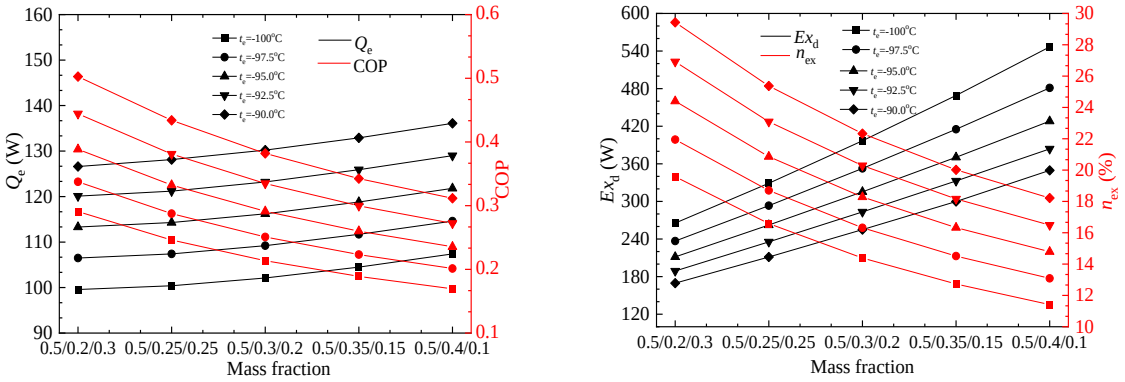

(a) Variations of Q_e and COP *(b) Variations of Ex_d and n_{ex}*

Fig. 4. Variations of output parameters with Z_{R1150} and Z_{R14} at different t_e

The vapor quality at the condenser outlet x_3 has great effects on the performance of the ACR system, and it is also an important parameter in the ACR's system. Thus, Fig. 5 shows the variations of Q_e, COP, E_{xd}, and n_{ex} with the Z_{R1150} changing from 0.2 to 0.4 under five vapor qualities at the condenser outlet x_3. It is found that Q_e and E_{xd} monotonically increase with increasing Z_{R1150}. However, COP and n_{ex} decrease. As shown in Fig. 5, Q_e, COP, and n_{ex} decrease, and E_{xd} increases under the different x_3. As the x_c increases, the refrigerant vapor that enters the condensation side of the cascade heat exchanger increases, and the refrigerant vapor is further condensed by two inner heat exchangers. The evaporator inlet vapor quality is increased as the x_9 and t_e are set to 0.4 and -100 ℃. Although the mass flow of the evaporator increases, Q_e still decreases (shown in Fig. 5c). What's more, when the Z_{R1150} is 0.4, p_{out}, p_{in}, and r_{com} are decreased as x_c increases, resulting in a reduction of W_{com}. Due to the faster decrease in the cooling capacity Q_e compared to the compressor power W_{com}. Therefore, the COP shows a decreasing trend. As the Z_{R1150} is 0.4, within the given x_c range (0.7~0.8), the COP, Q_{evap} and n_{ex} are decreased by 70.7 %, 71.43 %, and 70.77 %, and the E_{xd} is increased by 9.95 %.

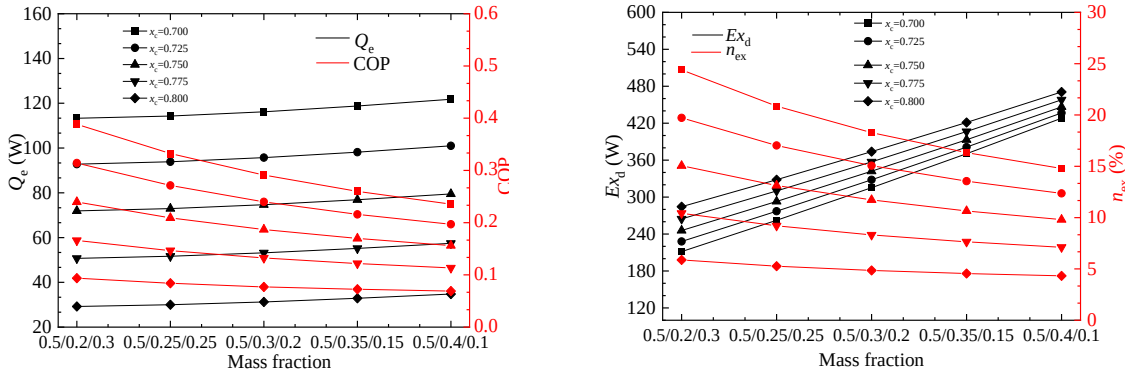

(a) Variations of Q_e and COP *(b) Variations of Ex_d and n_{ex}*

Fig. 5. Variations of output parameters with Z_{R1150} and Z_{R14} at different x_c

4.2. Performance at varying Z_{R600a} and Z_{R14}

Figure 6 reveals the effect of the Z_{R600a} and Z_{R14} at five t_c on Q_e, COP, E_{xd}, and n_{ex}. It is found from Fig. 6 that as the Z_{R600a} rises (or the Z_{R14} reduces), Q_e, COP, and n_{ex} of the ACR system indicate a downward trend, and E_{xd} monotonically increases. Actually, as the Z_{R14} decreases or the Z_{R600a} increases, the mass flow of low boiling point refrigerant decreases as the x_3 is set to 0.4, which affects the heat transfer of the cascade heat exchanger. It can be seen from Fig. 6b that the decrease rate of the p_{in} is greater than the p_{out}, resulting in an increase in the $r_{com,}$ which increases more significantly as the Z_{R600a} is larger than 0.5. When the t_e and x_e remain unchanged, Q_e decreases. Therefore, the increase in the Z_{R600a} results in an increase in the W_{com} and E_{xd}, and a decrease in the COP and n_{ex}. In addition, it is shown that the E_{xd} increases, and the COP, Q_e, and n_{ex} decrease as t_c increases. Since the t_3 ranges from 26 ℃~34 ℃, the COP, Q_e, and n_{ex} are decreased by 36.85~45.54 %, 23.09~31.95 %, 4.24~3.94 %, and 36.83~45.53 %, while E_{xd} are increased by 30.45~31.47 %.

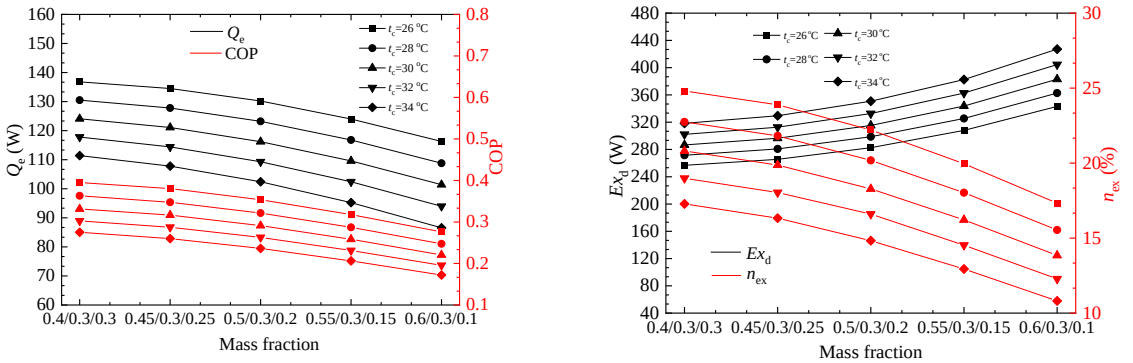

(a) Variations of Q_e and COP *(b) Variations of Ex_d and n_{ex}*

Fig. 6. Variations of output parameters with Z_{R600a} and Z_{R14} at different t_c

Figure 7 shows the variations in the performance of the ACR system with the Z_{R600a} and Z_{R14} at five t_e. It can be seen from Fig. 7 that Q_e, COP, and n_{ex} reduce linearly with the increment of the Z_{R600a}, and E_{xd} rises, and there is a minimum value for t_2 when the Z_{R600a} reaches 0.55. The results are consistent with the above results shown in Fig. 6. As the smaller value of R600a mass fraction (0.4), when the t_e decreases from -90 ℃ to -100 ℃, Q_e and COP vary in the ranges of 137~110.9 W and 0.4266~0.2496, the E_{xd} and n_{ex} vary in the ranges of 232~358.6 W, and 24.94~16.81%. The zeotropic mixture of R600a/R1150/R14 with a mass fraction of 0.4:0.3:0.3 obtaining the highest COP (0.4266)

at a t_e of -90 ℃ with a n_{ex} of 24.94 % is performing well. While the value of the R600a mass fraction is 0.6, within the given range of t_e, Other output parameters, such as Q_e, COP, E_{xd}, and n_{ex} do not vary obviously. It is noted that the increase of t_e can result in a higher saturation pressure, leading to a reduction of r_{com} when other parameters remain constant. Thus, W_{com} is decreased, and the COP and n_{ex} are increased.

Figure 8 reveals the effect of the Z_{R600a} and Z_{R14} on the performance of the ACR system under five x_3. As shown in Fig. 8, as the Z_{R600a} of the high boiling component increases from 0.4 to 0.6, the p_{in}, p_{out}, Q_e, COP, and n_{ex} decrease gradually. However, the decrease in p_{in} gradually slows down, while the decrease in p_{out} gradually accelerates. As the Z_{R600a} is greater than 0.45, the decrease rate of the p_{out} is larger than that of the p_{in}. Hence, the r_{com} of the ACR system first rises slowly and then increases rapidly, causing an increase in the W_{com}, and a decrease in the COP. Based on Eq. (6), the change trend of the n_{ex} is consistent with that of the COP (shown in Fig. 8d). Nevertheless, the t_2 decreases at first and then increases. It can also be seen that as the x_c rises, the Q_e, COP, p_{in}, p_{out}, and n_{ex} illustrate a downward trend, and the E_{xd} increases. As for t_2 and r_{com}, different variation trends exist when the mass fractions of R600a are different. As a smaller value of Z_{R600a} (0.4), the t_2 and r_{com} decrease with the x_c, but as a large value of 0.6, the trend of change is the opposite. Since the x_c varies from 0.7~0.8, within the given range of Z_{R600a}, the Q_e, COP, p_{in}, p_{out}, and n_{ex} are reduced by 61.03~91.11 %, 59.6~91.68 %, 16.31~22.34 %, 19.95~13.88 %, and 59.6~91.68 %, while the E_{xd} are increased by 12.1~23.23 %. However, the discharge temperatures of the compressor are still less than 120℃, ensuring the safety of the compressor.

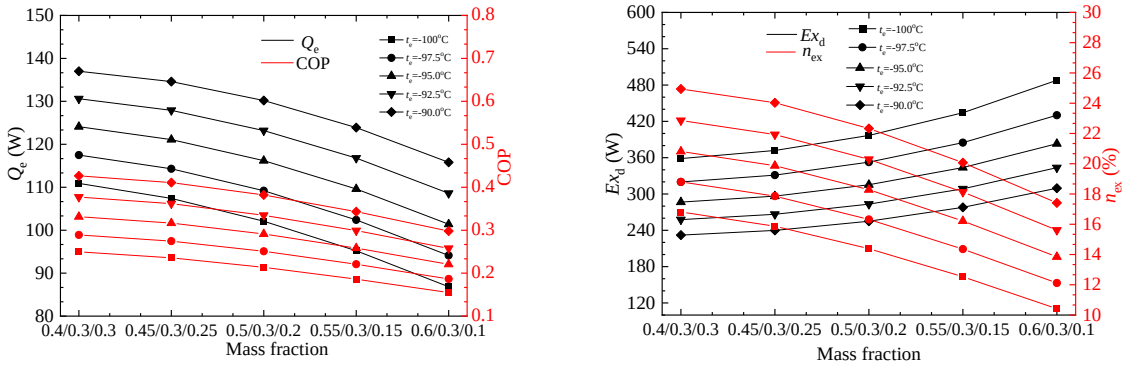

(a) Variations of Q_e and COP *(b) Variations of Ex_d and n_{ex}*

Fig. 7. Variations of output parameters with Z_{R600a} and Z_{R14} at different t_e

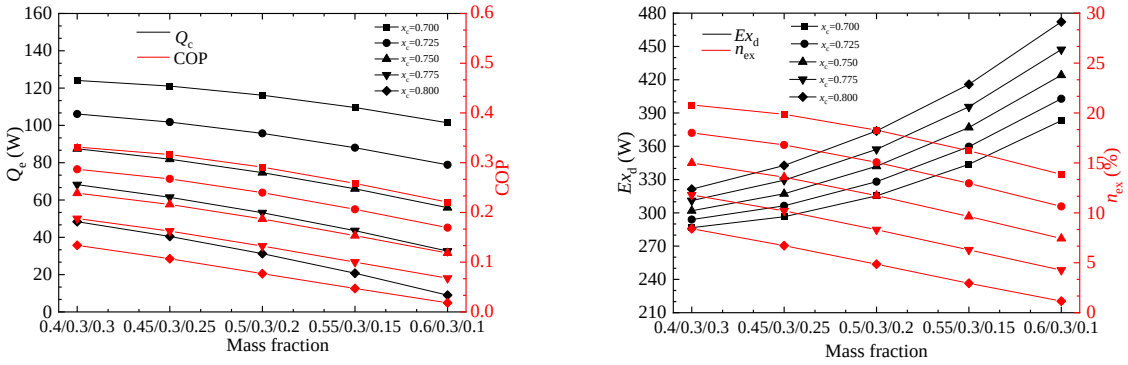

(a) Variations of Q_e and COP *(b) Variations of Ex_d and n_{ex}*

Fig. 8. Variations of output parameters with Z_{R600a} and Z_{R14} at different x_c

4.3. Performance at varying Z_{R600a} and Z_{R1150}

Figure 9 indicates the variation trend of the performance of the ACR system with Z_{R600a} and Z_{R1150} at different condensation temperatures. Under the calculation, the Z_{R14} and the vapor qualities at the condenser and evaporator outlets are 0.2, 0.7, and 0.4, respectively. As indicated in Fig. 9, as the Z_{R1150} mass fraction increases (or the Z_{R600a} decreases), the t_2, p_{in}, p_{out}, and Q_e increase in the form of a quadratic curve, the r_{com} and E_{xd} reduce first and then increase, while the COP and n_{ex} rise as the Z_{R1150} increases from 0.2~0.25 and then reduce gradually when the Z_{R1150} ranges from 0.25~0.40, meaning that the optimal values for the COP and n_{ex} exist. According to a comprehensive comparison and consideration, the value of 0.5 is selected as the optimum Z_{R1150} within the setting range of the condensation temperature $t_{c,}$ and the Z_{R600a}, Z_{R1150}, and Z_{R14} are 0.5:0.3:0.2. The corresponding maximum values of COP and n_{ex} under the t_3 of 26℃ are 0.3537 and 22.21%, respectively. In addition, as the condensation temperature increases, the performance of the ACR system shows a downward trend. When the Z_{R1150} is about 0.2 and the t_3 increases from 26~36 ℃, the t_2, r_{com}, Q_e, COP, E_{xd}, and n_{ex} vary from 88.59~111.7 ℃, 11.97~16.42, 103~67.68 W, 0.3023~0.1595, 271.3~360.1 W, and 18.98~10.02 %, respectively. When the Z_{R1150} reaches 0.4, the t_2 and r_{com} exceed the limited value. Simultaneously, Q_e, COP, and n_{ex} decreased by 23.29 %, 37.56 %, and 37.57 %, respectively.

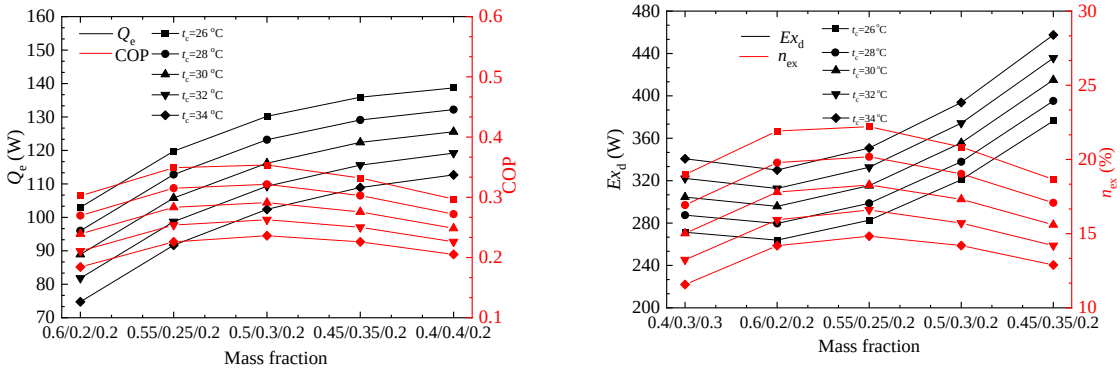

(a) Variations of Q_e and COP *(b) Variations of Ex_d and n_{ex}*

Fig. 9. Variations of output parameters with Z_{R600a} and Z_{R1150} at different t_c

Figure 10 presents the impact of the Z_{R600a} and Z_{R1150} on the performance of the ACR system at different evaporator temperatures. It can also be seen that the parameters, including Q_e, increase monotonically with increasing Z_{R1150}. However, when the Z_{R1150} is about 0.3 and t_e is a larger value of -90℃, the optimal values of COP, E_{xd}, and n_{ex} are 0.382, 255.0 W, and 22.33 %, respectively. Meanwhile, when the Z_{R1150} is constant, Q_e, COP, and n_{ex} monotonically increase with the growth of t_e, and the E_{xd} increases. As mentioned above, the increase of t_e will result in the decrease of r_{com}, thus W_{com} decreases and COP increases (shown in Fig. 10a). As seen in Fig. 10a and Fig. 10b, Q_e, COP, and n_{ex} are increased by 37.18 %, 93.62 %, and 68.02 % with the increase of the t_e as Z_{R1150} is 0.2. Nevertheless, Q_e, COP, and n_{ex} are increased by 23.91 %, 78.85 %, and 55.27 % when the Z_{R1150} is 0.4, indicating that an increase in evaporation temperature can improve the performance of the ACR system quickly with a small Z_{R1150}. However, the performance of the system is influenced by various factors, and the comprehensive consideration of multiple factors should be taken into consideration.

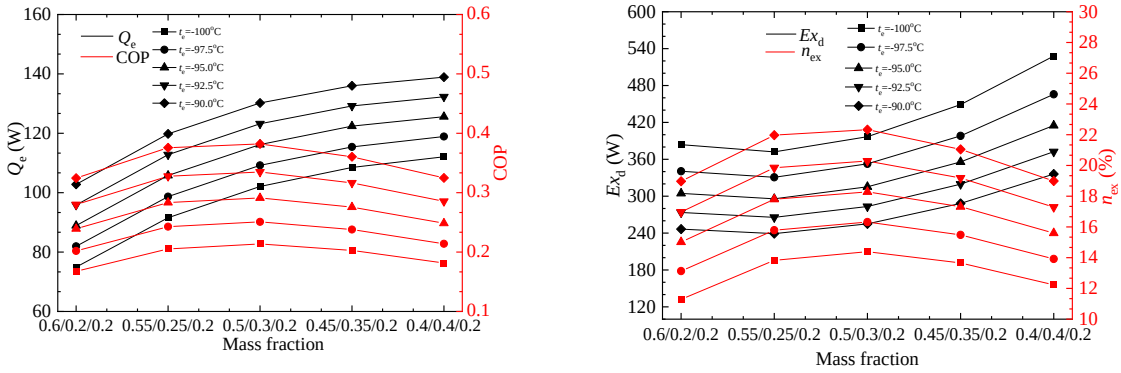

(a) Variations of Q_e and COP *(b) Variations of Ex_d and n_{ex}*

Fig. 10. Variations of output parameters with Z_{R600a} and Z_{R1150} at different t_e

Figure 11 shows the variations in the ACR's performance with the Z_{R600a} and Z_{R1150} at different vapor qualities at the condenser outlet x_3. It can be found that Q_e increases linearly first, then slowly. However, there are optimal values for E_{xd}, COP, and n_{ex} when the Z_{R600a}, Z_{R1150}, and Z_{R14} are 0.5, 0.3, and 0.2, respectively. As for the trend of change of the t_2, it can be seen that in the case of x_c=0.7, It is clearly observed that the increase in the x_c has adverse effects on the performance of the ACR system. When the Z_{R1150} is 0.2, the Q_e, COP, and n_{ex} are decreased by 97.08 %, 97.50 %, and 97.43 % respectively, within the given range of the x_c. But the corresponding parameters are reduced by 61.78 %, 59.43 %, and 59.44 % as the Z_{R1150} is 0.4, indicating that the x_c has a more significant impact on the ACR's performance as a smaller value of the Z_{R1150}.

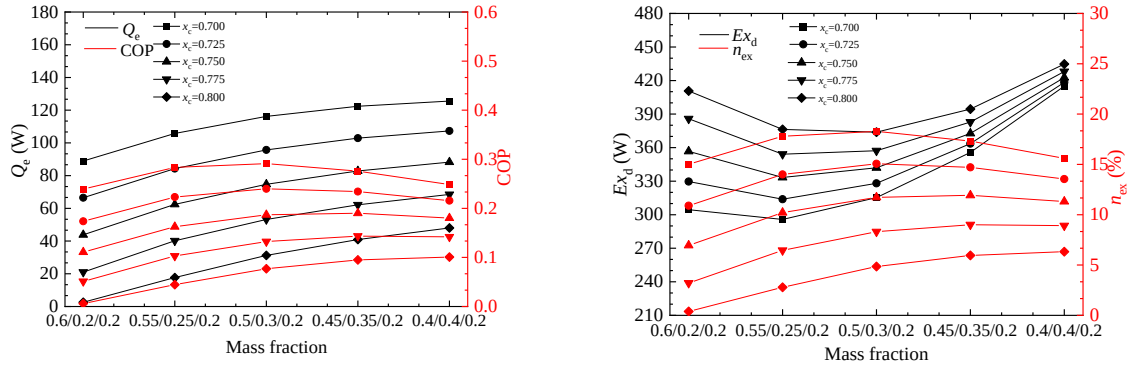

(a) Variations of Q_e and COP *(b) Variations of Ex_d and n_{ex}*

Fig. 11. Variations of output parameters with Z_{R600a} and Z_{R1150} at different x_c

4.4. Analysis of grey correlation degree

According to the calculation results in Figs. 3- 11, the results of the grey correlation degree are calculated in Fig. 12. In Fig. 12, states 1~3 present the situation when the Z_{R600a}, Z_{R1150}, and Z_{R14} remain unchanged, respectively, while the other two working fluid components change separately. It can be found that the degree of grey correlation between the three states and Q_e and p_{out} are mainly determined by state 1, but COP and n_{ex} are controlled by state 3.

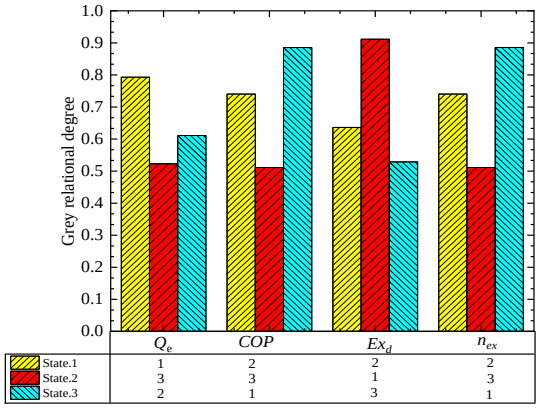

Fig. 12. Grey relational degree and order (table) between three states and output parameters

5. Conclusions

A theoretical model was built to analyze the energy and exergy performance of an ACR system using R600a/R1150/R14 with different initial mass fractions of the refrigerants and operating conditions. The correlation degrees between different states and the output parameters were obtained by using the grey correlation theory. The following conclusions were made:

(1) Under the Z_{R600a} of 0.5, as the Z_{R1150} was increased from 0.2 to 0.4 (state 1), the cooling capacity and total exergy destruction rates increased, and the COP and exergy efficiency decreased. The performance increased with the rising evaporation temperature, the decreasing condensation temperature, and the vapor quantity at the condenser outlet. The mixture of R600a/R1150/R14 with a mass fraction of 0.5:0.2:0.3 having COP of 0.5027 and 29.43 % of exergy efficiency under the condensation temperature and evaporation temperature of 30 ℃ and -90 ℃ was recommended.

(2) When the Z_{R1150} was set to be 0.3, with the increasing Z_{R600a} (state 2), the total exergy destruction rates increased, but the cooling capacity, COP, and exergy efficiency decreased. At an evaporation temperature of -90 ℃, a condensation temperature of 30 ℃, a vapor quantity of the condenser outlet of 0.7, the mixture of R600a/R1150/R14 with a mass fraction of 0.4:0.3:0.3 having cooling capacity of 137.0 W, COP of 0.4266, and 24.94 % of exergy efficiency was performing well.

(3) As the Z_{R14} was unchanged but the Z_{R1150} and Z_{R600a} varied (state 3) under different operating conditions, the highest COP and exergy efficiency were found with the mass fraction of 0.5:0.3:0.2 for the mixture of R600a/R1150/R14. What's more, the effects of the evaporation temperature on the ACR's performance were more obvious than those of the condensation temperature and the vapor quantity of the condenser outlet.

(4) Through the correlation degree analysis between each state (varying Z_{R600a}, Z_{R1150}, and Z_{R14}) and the performance evaluating output parameters, the factor that had the greatest impact on the cooling capacity was state 1, followed by state 3, while state 2 had the least impact. But state 2 had the greatest effect on the pressure ratio, suction pressure of the compressor, and total exergy destruction rate, and the exergy efficiency and COP were most affected by state 3.

In summary, the theoretical research findings obtained thus provide a clear roadmap for conducting further experimental investigations. Additionally, the utilization of the grey correlation theory could offer advantages for the performance improvement of the ACR system. In our future research, the calculation results will be tested and verified under an experimental condition. Besides, the analysis of thermodynamic performance, coupled with experimental results, will enhance the

applicability of the gray correlation theory presented in this paper.

Nomenclature

Ex_d	exergy destruction rate [W]
h	specific enthalpy [kJkg^{-1}]
m	mass flow rate [kgs^{-1}]
n	exergy efficiency [%]
p	pressure [MPa]
Q	heat load [W]
r	pressure ratio
s	specific entropy[kJkg^{-1}K^{-1}]
t/T	temperature [℃]
W	compressor input power [W]
x	vapor quality of two-phase flow [kg·kg^{-1}]
Z	mass fraction

Subscripts

0	reference state
1-14	state points of refrigerant
com	compressor
cond/c	air-cooled condenser
CHX	cascade heat exchanger
evap/e	evaporator
exp	expansion valve
in	inlet
is	isentropic
IHX	internal heat exchanger
out	outlet

Greek symbols

η_{com}	isentropic efficiency of the compressor
Δt	temperature difference [℃]

Acknowledgements

This work is financially supported by the National Natural Science Foundation of China (No. 52106027), Hongliu Excellent Youth Talent Program Project of Lanzhou University of Technology (2023), and Changzhou Applied Basic Research Program (CJ20220215).

References

[1] Johnson, N., *et al.,* Design and control of a cryogenic multi-stage compression refrigeration process, *Chemical Engineering Research and Design, 121* (2017), pp. 360-367

[2] Pan, Z., *et al.,* A Review of the Cascade Refrigeration System, *Energies, 2254* (2020), 13, pp. 3-26

[3] Zhang, Y. Q., *et al.,* Experimental investigation of the performance of an R1270/CO_2 cascade refrigeration system, *International Journal of Refrigeration, 114* (2020), pp. 175-180

[4] Sholahudin, S., Giannetti, N., Optimization of a cascade refrigeration system using refrigerant C_3H_8 in high temperature circuits (HTC) and a mixture of C_2H_6/CO_2 in low temperature circuits (LTC), *Applied Thermal Engineering, 104* (2016), pp. 96-10

[5] Xu, X. W., *et al.,* Mixed refrigerant composition shift due to throttle valves opening in auto cascade refrigeration system, *Chinese Journal of Chemical Engineering, 23* (2015), pp. 199-204

[6] Liu. Y., *et al.,* Theoretical analysis of a double ejector-expansion auto-cascade refrigeration cycle using hydrocarbon mixture R290/R170, *International Journal of Refrigeration, 94* (2018), pp. 33-39

[7] Cheng, Z., *et al.,* Performance evaluation of novel double internal auto-cascade two-stage compression system using refrigerant mixtures, *Applied Thermal Engineering, 168* (2020), 114898

[8] Wang, Q., *et al.*, Numerical investigations on the performance of a single-stage auto- cascade refrigerator operating with two vapor–liquid separators and environmentally benign binary refrigerants, *Applied Energy, 112* (2013), pp. 949-955
[9] Sivakumar, M., Somasundaram, P., Exergy and energy analysis of three stage auto refrigerating cascade system using zeotropic mixture for sustainable development, *Energy Conversion and Management, 84* (2014), pp. 589-596
[10] Rui, S., *et al.*, Experimental investigation of the performance of a single-stage auto-cascade refrigerator, *Heat Mass Transfer, 52* (2016), pp. 11-20
[11] Qin, Y. B., *et al.*, Thermodynamic performance of a modified -150 ◦C refrigeration system coupled with Linde-Hampson and three-stage auto-cascade using low-GWP refrigerants, *Energy Conversion and Management, 236* (2021), 114093
[12] Liu, J. R., *et al.*, Thermodynamic analysis of a novel ejector-enhanced auto-cascade refrigeration cycle, *Applied Thermal Engineering, 200* (2022), 117636
[13] Rodríguez-Jara, E. A., *et al.*, Thermodynamic analysis of auto-cascade refrigeration cycles, with and without ejector, for ultra-low temperature freezing using a mixture of refrigerants R600a and R1150, *Applied Thermal Engineering, 200* (2022), 117538
[14] Liu, F. Z., *et al.*, Performance evaluation of an auto-cascade refrigeration system using grey correlation theory and response surface methodology, *Science and Technology for the Built Environment, 0* (2023), pp. 1-17
[15] Ye, W. L., *et al.* Application of response surface methodology and desirability approach to optimize the performance of an ultra-low temperature cascade refrigeration system, *Applied* Thermal Engineering, *239* (2024), 122130
[16] Elakdhar, M., *et al.*, Analysis of a compression/ejection cycle for domestic refrigeration, *Industrial & Engineering Chemistry Research, 46* (2007), 130, pp. 4639-4644
[17] Li, M., Grey correlation analysis of low-carbon governance in Yangtze River delta cities, *Journal of Environmental and Public Health,* (2022), 2029087
[18] Li, C., *et al.*, Multi-objective optimization strategy based on entropy weight, grey correlation theory, and response surface method in turning, *International Journal of Industrial Engineering, 28* (2021), 5, pp. 490-507

Submitted: 23.01.2024.

Revised: 07.04.2024.

Accepted: 11.04.2024.